

Supplementary Material: Modulating the Graphitic Domains of Hard Carbons via Tuning Resin crosslinking Degree to Achieve High Rate and Stable Sodium Storage

We report a hard carbon (HC) material derived from 3-aminophenol formaldehyde resin (AFR) with better rate performance, higher initial coulombic efficiency (ICE) and capacity via adjusting the crosslinking degree of the AFR precursor. We discover that a resin precursor with a higher crosslinking degree tends to produce HC with higher carbon yield, a larger d_{002} , fewer defects, and a lower surface area.

MAIN TEXT

Supplementary Table 1. Physical parameters for 0.46-AFR-HC, 0.90-AFR-HC and 1.80-AFR-HC.

		0.46-AFR-HC	0.90-AFR-HC	1.80-AFR-HC
TEM	d_{002} (nm)	0.388	0.384	0.372
	L_c (nm)	1.40	1.36	1.32
	L_a (nm)	2.64	2.59	2.54
XRD	d_{002} (nm)	0.401	0.389	0.374
	L_c (nm)	1.46	1.42	1.33
	L_a (nm)	3.01	2.89	2.88

$d_{002} = n\lambda/2\sin\theta = 0.154187/2\sin\theta$, $L = K\gamma/B\cos\theta$, $N = Lc/d_{002} + 1$, K is the Scherrer constant (usually set as 0.98), γ is the wavelength of the X-ray beam, B is the full width at half maximum (FWHM) value of the (002) and (100) peak, 2θ is the diffraction angle, and L is the average thickness in the per-pendicular direction of the crystal plane; L_a : the apparent layer-plane length parallel to the fiber axis; L_c : the apparent crystallite thickness; d_{002} : the average interlayer distance.^[S1-S3]

© The Author(s) 2021. Open Access This article is licensed under a Creative Commons Attribution



4.0 International License (<https://creativecommons.org/licenses/by/4.0/>), which permits unrestricted use, sharing, adaptation, distribution and reproduction in any medium or

format, for any purpose, even commercially, as long as you give appropriate credit to the original author(s) and the source, provide a link to the Creative Commons license, and indicate if changes were made.



Supplementary Table 2. Raman parameters for 0.46-AFR-HC, 0.90-AFR-HC and 1.80-AFR-HC.

	I _D	I _G	I _D /I _G
0.46-AFR-HC	0.9491	0.9968	0.95
0.90-AFR-HC	0.9723	0.9815	0.99
1.80-AFR-HC	0.9989	0.9561	1.04

Supplementary Table 3. Pore structure and specific surface area information for 0.46-AFR-HC, 0.90-AFR-HC and 1.80-AFR-HC.

N ₂	BET Surface Area (m ² /g)	CO ₂	Micropore Surface Area (m ² /g)
0.46-AFR-HC	11.1750	0.46-AFR-HC	506.4595
0.90-AFR-HC	35.7286	0.90-AFR-HC	518.7026
1.80-AFR-HC	52.8906	1.80-AFR-HC	634.4605

Supplementary Table 4. Atomic ratios of elements C, N, and O in 0.46-AFR-HC, 0.90-AFR-HC and 1.80-AFR-HC from XPS

	C (at%)	N (at%)	O (at%)
0.46-AFR-HC	93.29	1.27	5.36
0.90-AFR-HC	92.63	1.28	5.98
1.80-AFR-HC	92.07	1.44	6.4

Supplementary Table 5. The compaction density of 0.46-AFR-HC, 0.90-AFR-HC and 1.80-AFR-HC.

	Compaction density (g/cm ³)
0.46-AFR-HC	0.82
0.90-AFR-HC	0.79
1.80-AFR-HC	0.75

Supplementary Table 6. Summary of representative publications with high capacity of HC and other anode materials previously reported in the literature.

Materials	Capacity (mAh g ⁻¹)	Rate capability (mAh g ⁻¹)	Temperature (°C)	Ref
Seedpod-HC	328	85 @ 1 A g ⁻¹	1200	[S4]
Pitch-C	250	124 @ 10 A g ⁻¹	1000	[S5]
O-Carbon	380	152 @ 2 A g ⁻¹	1600	[S6]
N-HC	364	214 @ 10 A g ⁻¹	1200	[S7]
HC	320	80 @ 5 C	1200	[S8]
Pitch and Resin-HC	350	145 @ 20 A g ⁻¹	1000	[S9]
Cu-carbon microcuboid	201	136 @ 2 A g ⁻¹	600	[S10]
0.46-AFR-HC	383	140 mAh g ⁻¹ @ 20 A g ⁻¹	1300	This work

1. **Supplementary Table 7.** Summary of representative publications with high ICE of HC previously reported in the literature.

Materials	ICE (%)	Electrolyte	Ref
HCNS	82	1 M NaPF ₆ in diglyme	[S7]
HC-1	79	1 M NaPF ₆ in TEGDME	[S8]
Pitch and Resin-HC	63	1 M NaPF ₆ in diglyme	[S9]
Cu-carbon microcuboid	60	1 M NaCF ₃ SO ₃ in diglyme	[S10]
HC-2	75	1 M NaPF ₆ in diglyme	[S2]
0.46-AFR-HC	82	1 M NaPF ₆ in diglyme	This work

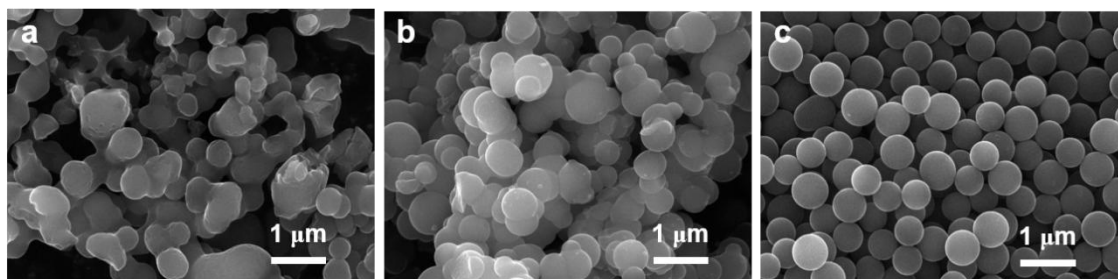
Supplementary Table 8. EIS fitting data for 0.46-AFR-HC, 0.90-AFR-HC and 1.80-AFR-HC electrodes.

Samples	Cycles	R_s	R_{SEI}	R_{ct}
0.46-AFR-HC	10	10.3	2.6	3.6
0.90-AFR-HC	10	10.2	3.8	7.7
1.80-AFR-HC	10	10.4	7.3	11.8

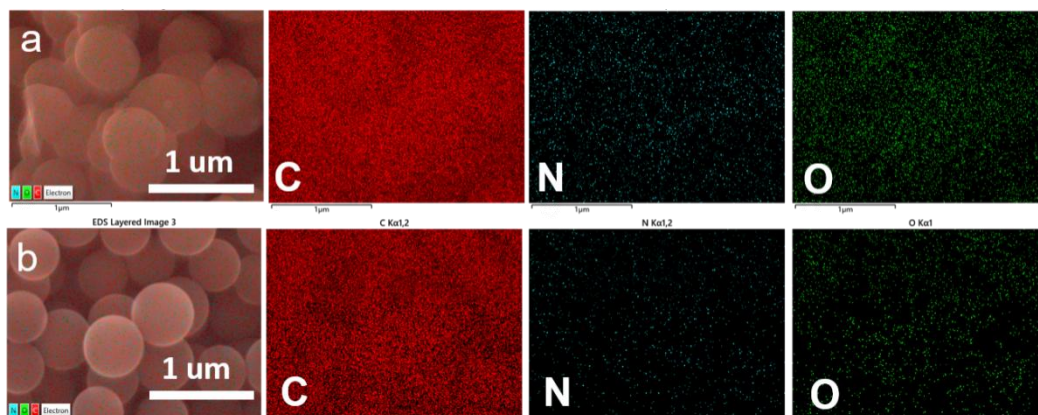
R_s : internal resistance including the resistances of the electrolyte solution and electrodes;

R_{SEI} : interfacial resistance of electrode due to formation of SEI;

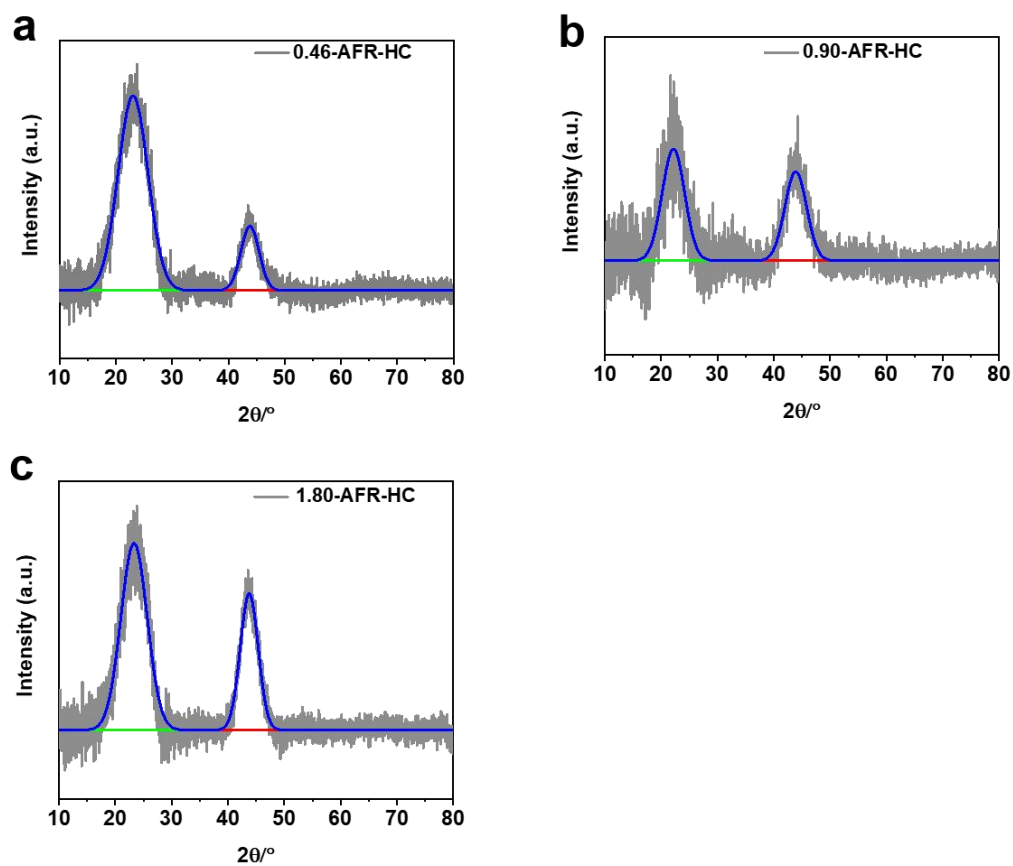
R_{ct} : resistance associated with charge transfer.



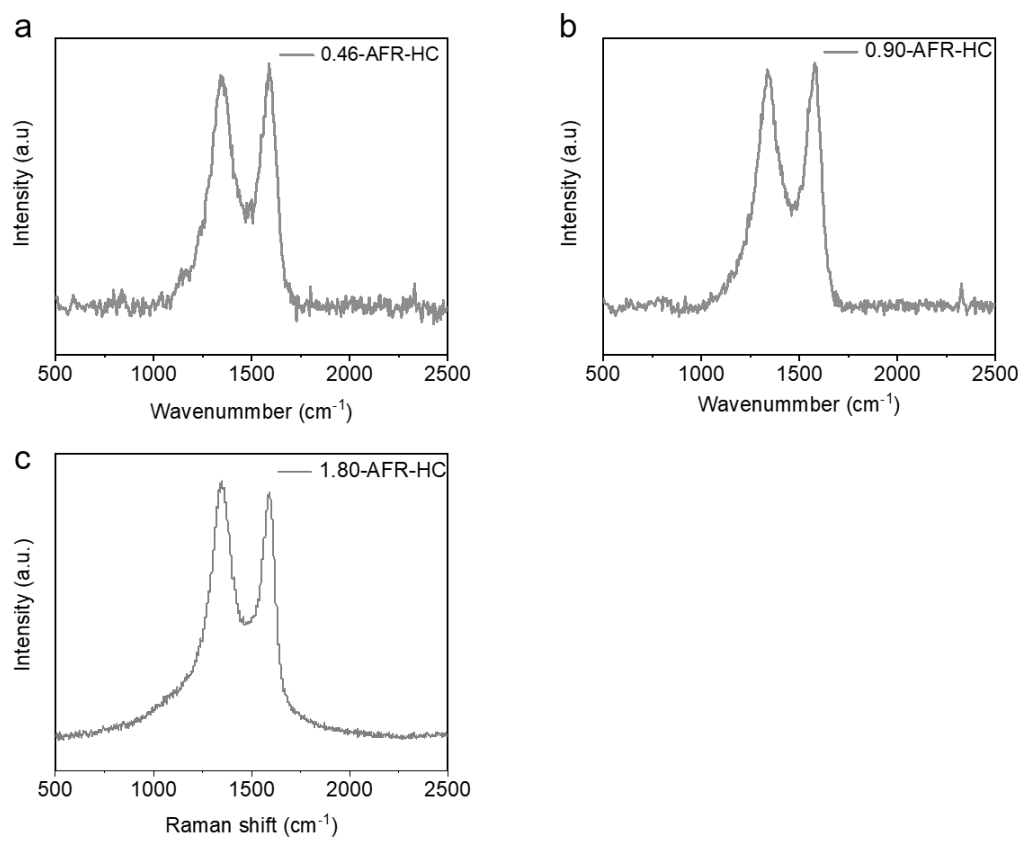
Supplementary Figure 1. SEM images for (a) 0.46-AFR-HC, (b) 0.90-AFR-HC and (c) 1.80-AFR-HC.



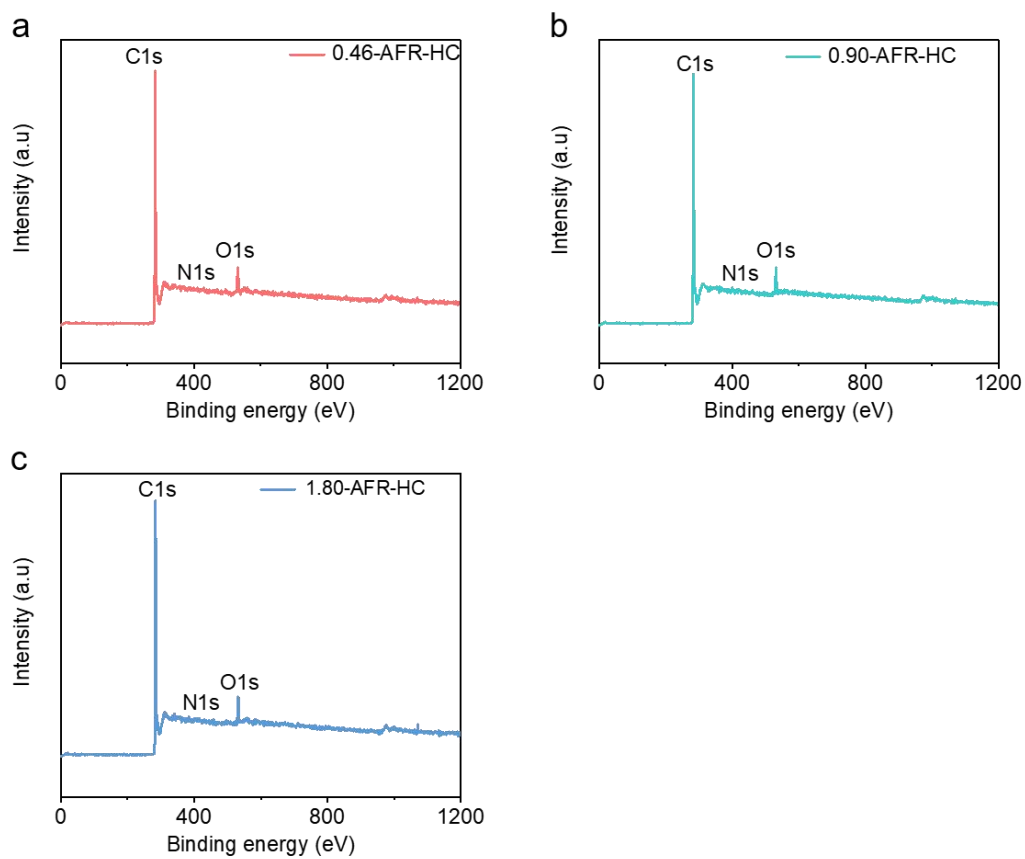
Supplementary Figure 2. Energy dispersive spectrometer mappings for (a) 90-AFR-HC and (b) 1.80-AFR-HC.



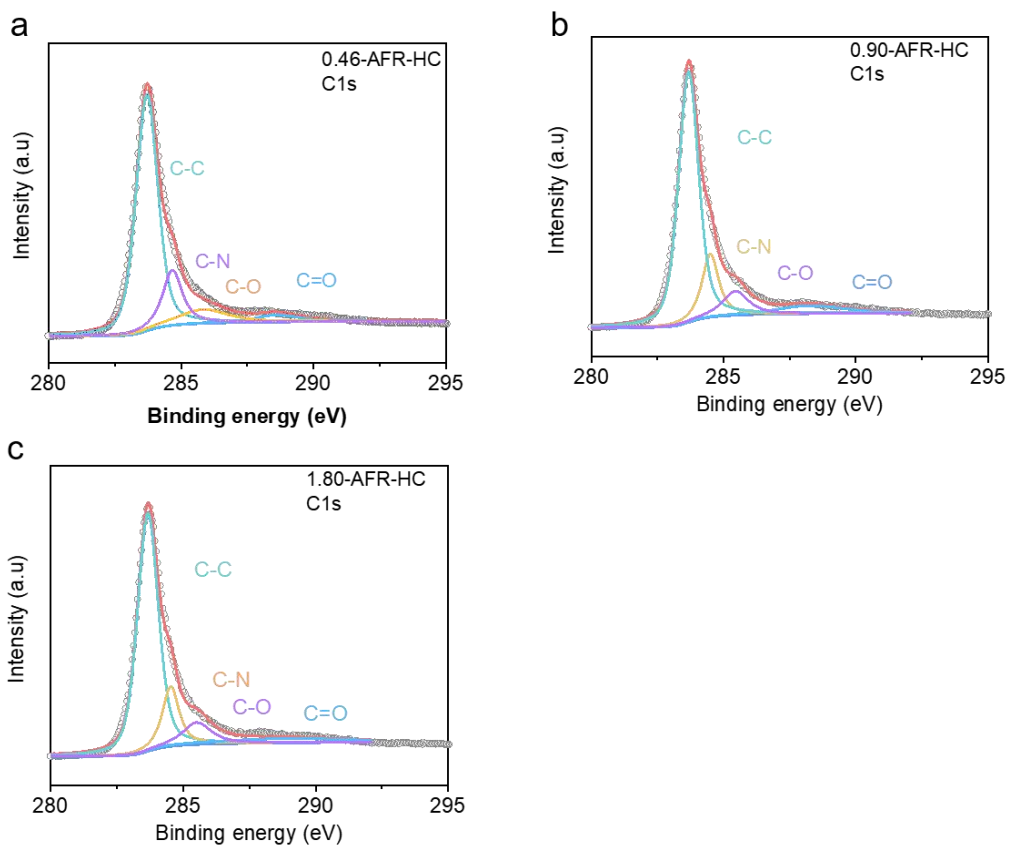
Supplementary Figure 3. XRD patterns. (a) 0.46-AFR-HC, (b) 0.90-AFR-HC and (c) 1.80-AFR-HC.



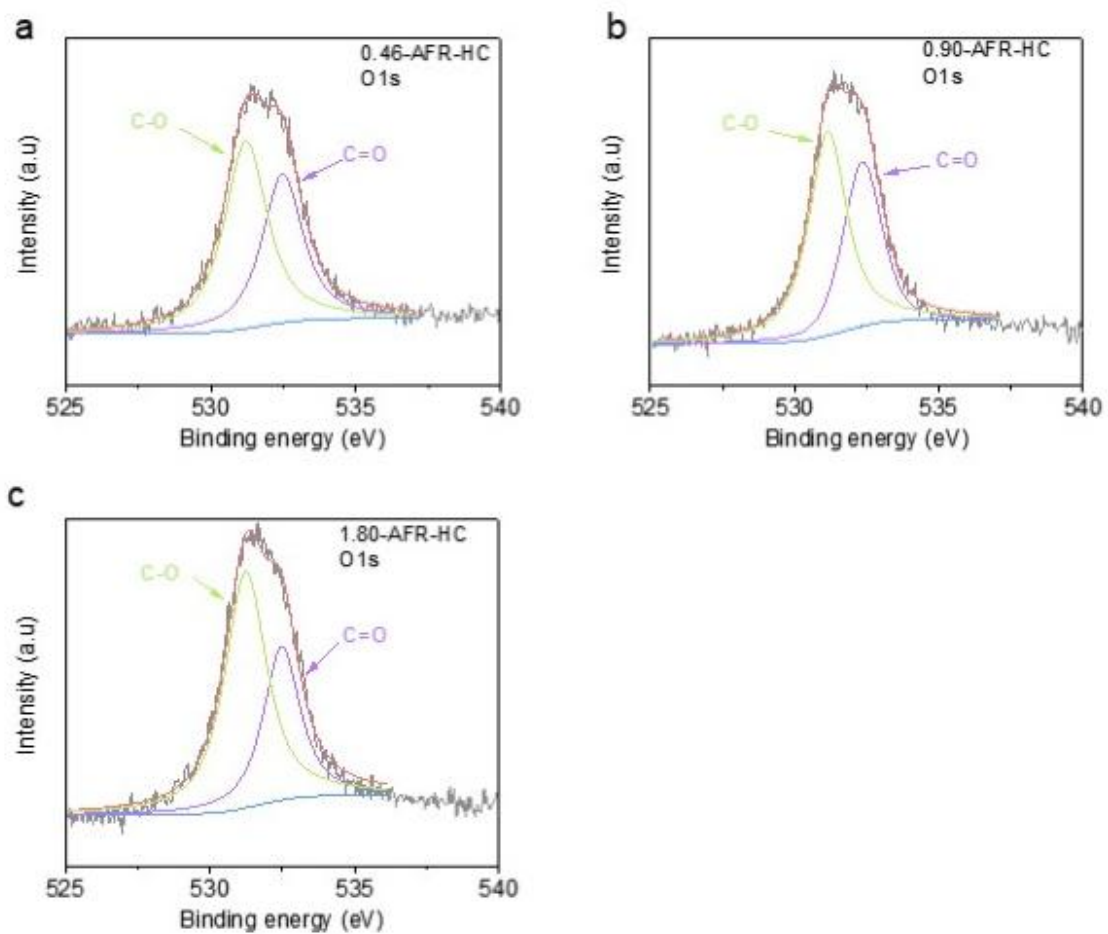
Supplementary Figure 4. Raman spectra. (a) 0.46-AFR-HC, (b) 0.90-AFR-HC and (c) 1.80-AFR-HC.



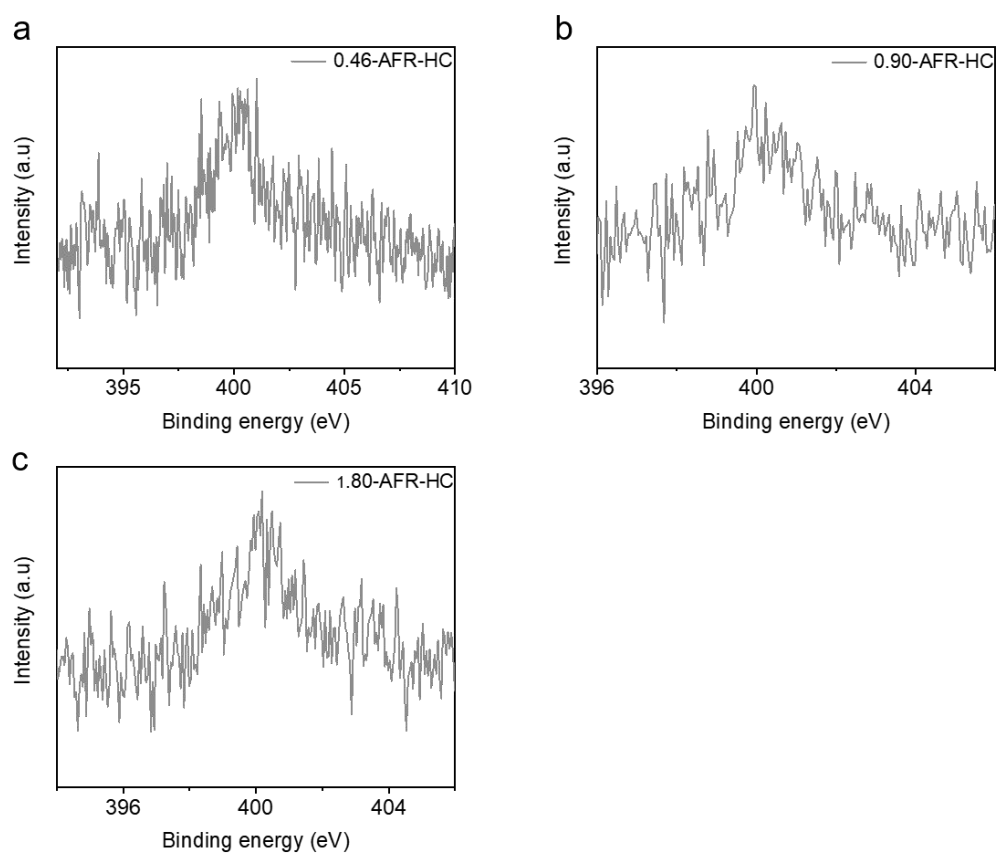
Supplementary Figure 5. The full XPS spectra. (a) 0.46-AFR-HC. (b) 0.90-AFR-HC. (c) 1.80-AFR-HC.



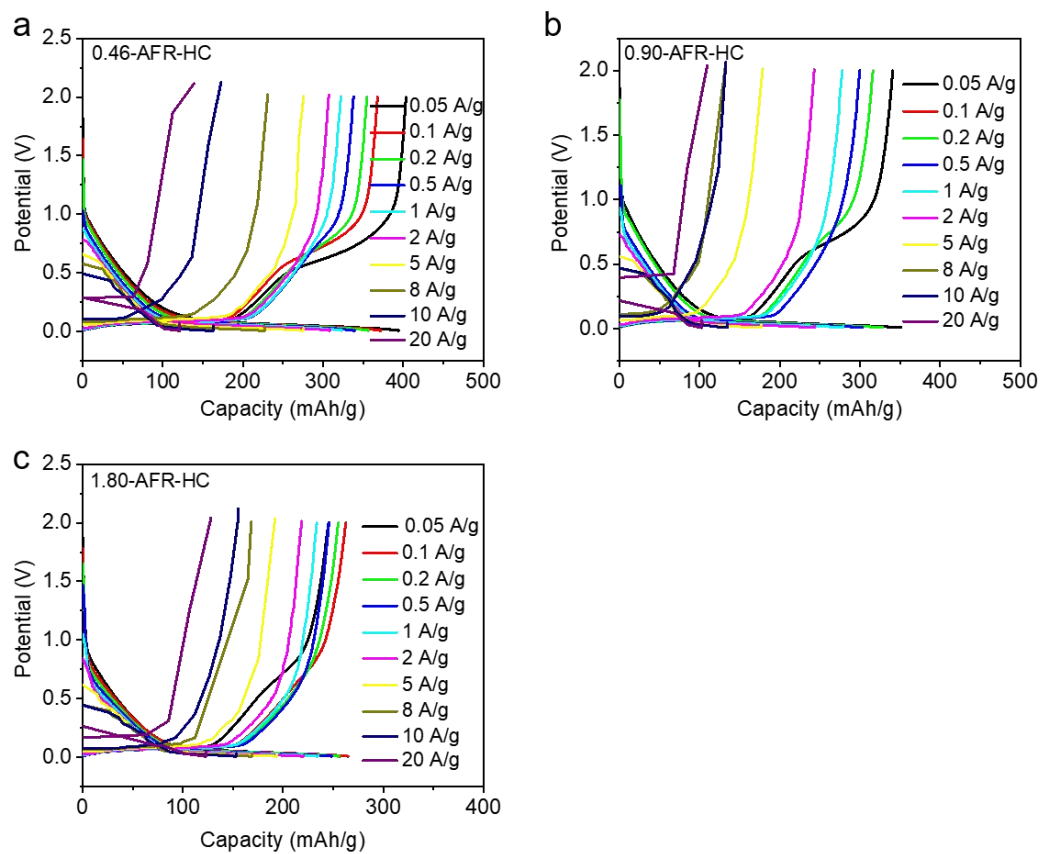
Supplementary Figure 6. The high-resolution XPS of C 1s spectra. (a) 0.46-AFR-HC. (b) 0.90-AFR-HC. (c) 1.80-AFR-HC.



Supplementary Figure 7. The high-resolution XPS of O 1s spectra. (a) 0.46-AFR-HC. (b) 0.90-AFR-HC. (c) 1.80-AFR-HC.

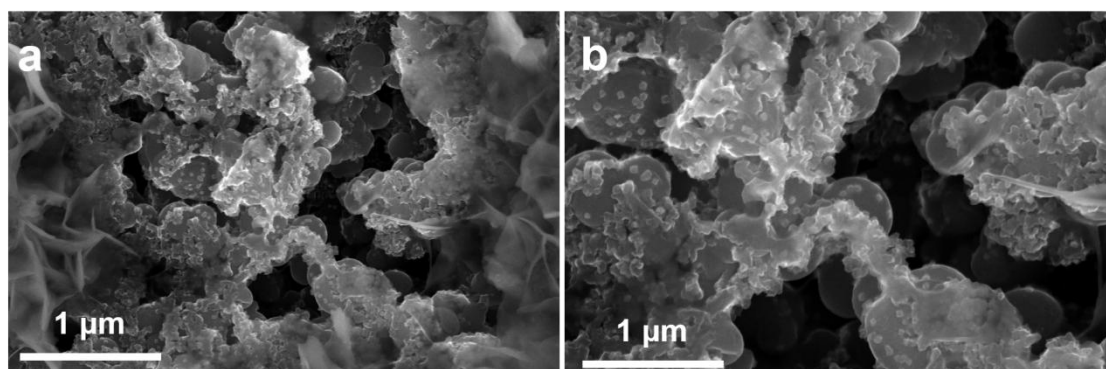


Supplementary Figure 8. The high-resolution XPS of N 1s spectra. (a) 0.46-AFR-HC. (b) 0.90-AFR-HC. (c) 1.80-AFR-HC.

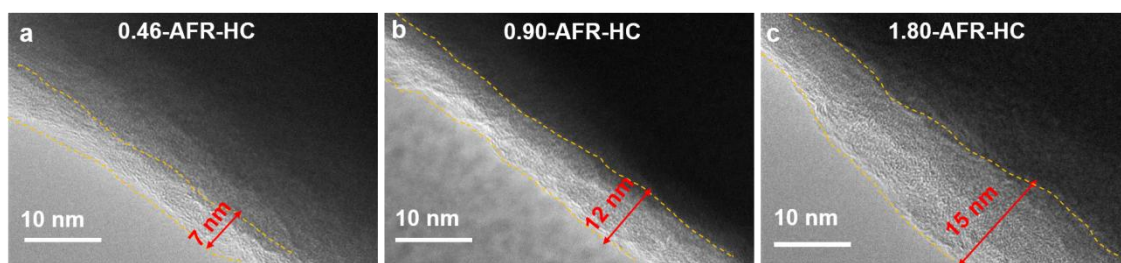


Supplementary Figure 9. The discharge-charge curves at different current densities (a)

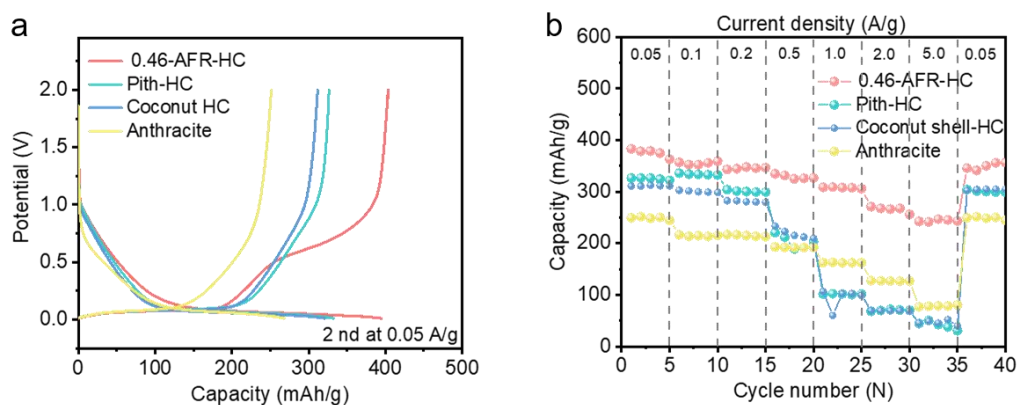
0.46-AFR-HC. (b) 0.90-AFR-HC. (c) 1.80-AFR-HC.



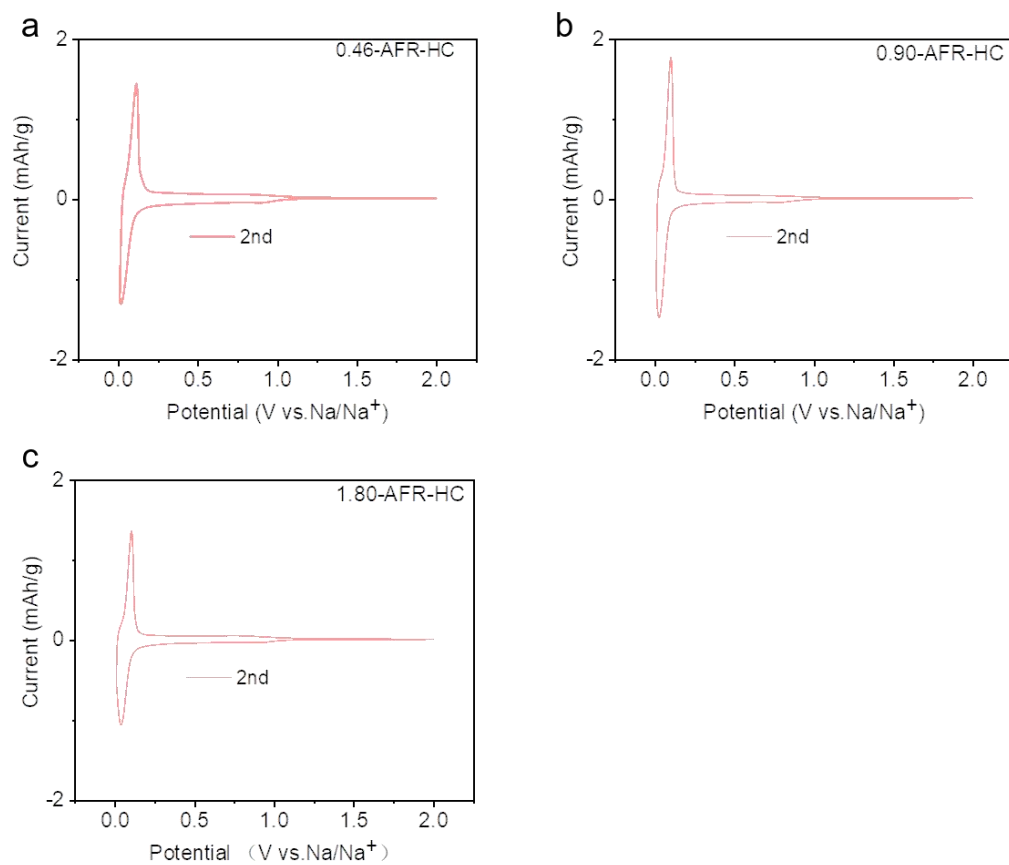
Supplementary Figure 10. (a-b) SEM images of 0.46-AFR-HC electrodes (0.1 A g^{-1} , 100th cycle, $25 \text{ }^{\circ}\text{C}$).



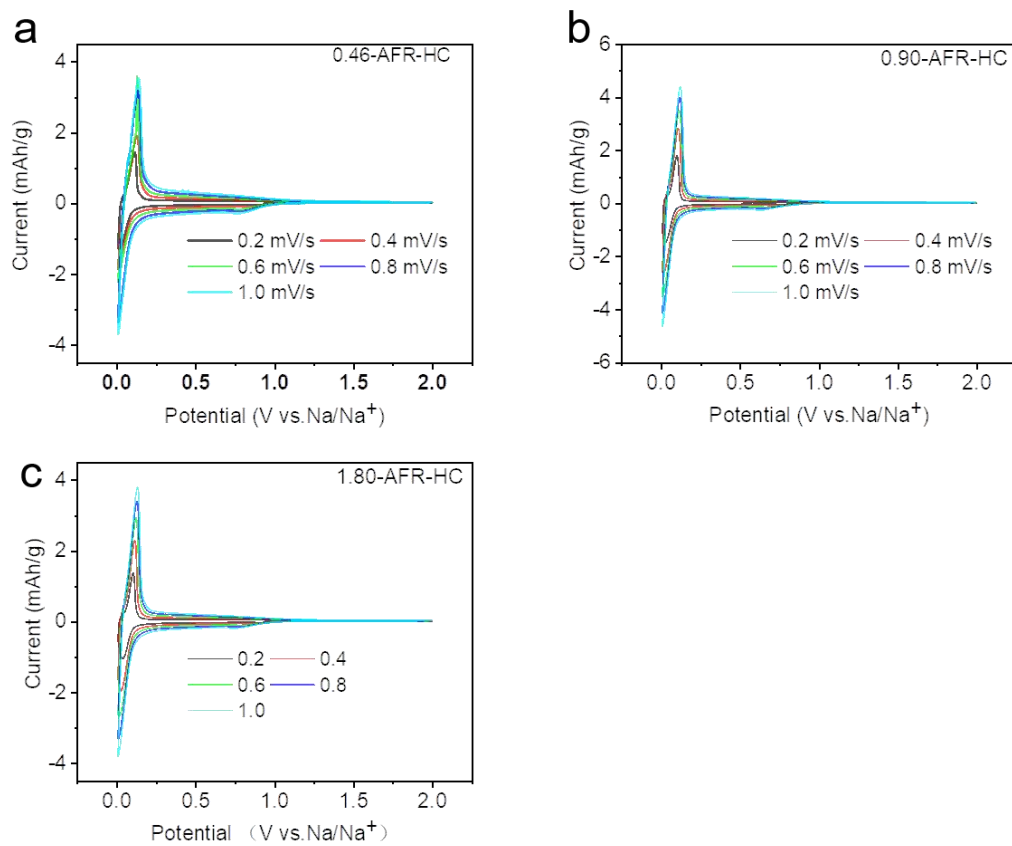
Supplementary Figure 11. HRTEM images of 0.46-AFR-HC (a), 0.90-AFR-HC (b) and 1.80-AFR-HC (c) electrodes (0.1 A g^{-1} , 50th cycle, $25 \text{ }^\circ\text{C}$).



Supplementary Figure 12. (a) The GCD curves (the second cycle) of different hard carbons. (b) Rate performance of different types hard carbons.

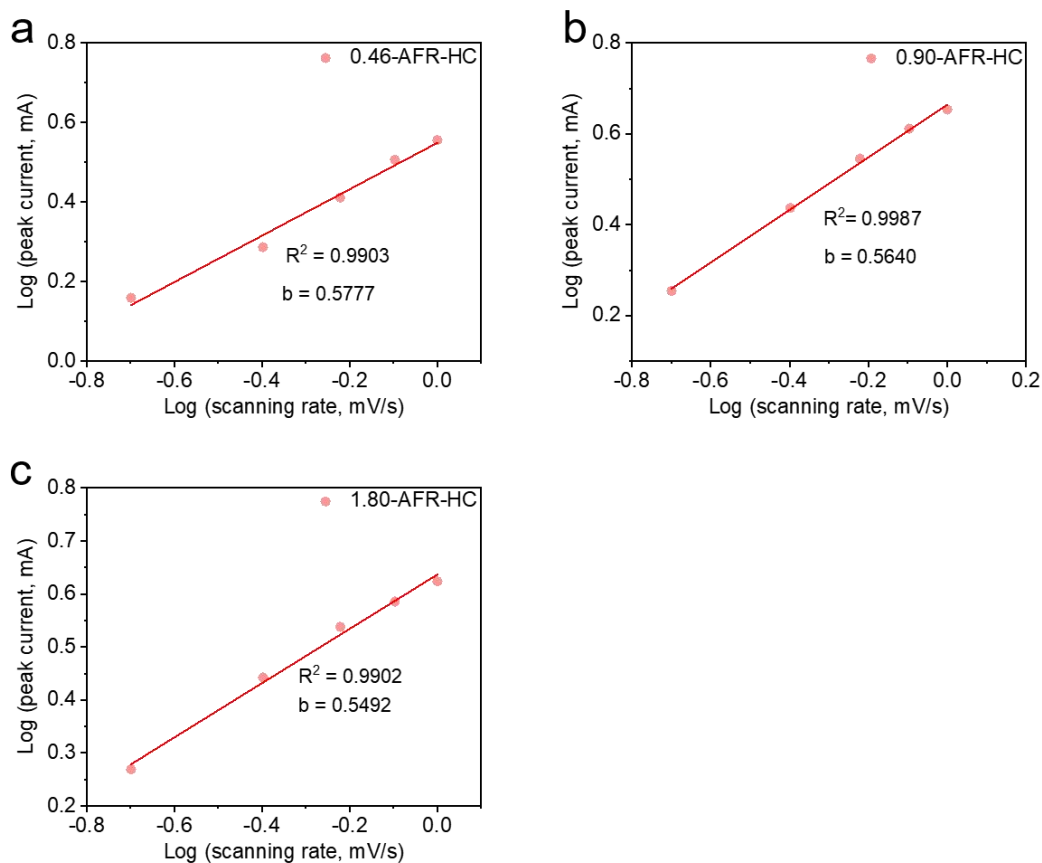


Supplementary Figure 13. Cyclic voltammety curves at scan rates of 0.2 mV s⁻¹. (a) 0.46-AFR-HC. (b) 0.90-AFR-HC. (c) 1.80-AFR-HC.



Supplementary Figure 14. CV curves at different scan rates of 0.2-1.0 mV s⁻¹. (a) 0.46-AFR-HC.

(c) 0.90-AFR-HC. (b) 1.80-AFR-HC.



Supplementary Figure 15. Fitting results of b value for (a) 0.46-AFR-HC, (b) 0.90-AFR-HC and (c) 1.80-AFR-HC electrodes.

REFERENCES

- [S1] Wen Y, He K, Zhu Y, et al. Expanded graphite as superior anode for sodium-ion batteries. *Nat Commun* 2014;5:4033. [DOI: 10.1038/ncomms5033]
- [S2] Yin X, Lu Z, Wang J, et al. Enabling Fast Na⁽⁺⁾ transfer kinetics in the whole-voltage-region of hard-carbon anodes for ultrahigh-rate sodium storage. *Adv Mater* 2022;34(13):2109282. [DOI: 10.1002/adma.202109282]
- [S3] Lu Z, Wang J, Feng W, et al. Zinc Single-atom regulated hard carbons for high rate and low temperature sodium ion batteries. *Adv. Mater.* 2023;35:2211461. [DOI: 10.1002/adma.202211461]
- [S4] Wu F, Zhang M, Bai Y, Wang X, Dong R, Wu C. Lotus seedpod-derived hard carbon with hierarchical porous structure as stable anode for sodium-ion batteries. *ACS Applied Materials & Interfaces* 2019;11 (13):12554. [DOI: 10.1021/acsami.9b01419]
- [S5] Hao M, Xiao N, Wang Y, et al. Pitch-derived N-doped porous carbon nanosheets with expanded interlayer distance as high-performance sodium-ion battery anodes. *Fuel Processing Technology* 2018;177:328. [DOI: 10.1016/j.fuproc.2018.05.007]
- [S6] Sun F, Wang H, Qu Z, et al. Carboxyl-dominant oxygen rich carbon for improved sodium ion storage: synergistic enhancement of adsorption and intercalation mechanisms. *Adv. Energy Mater.* 2020;11(1):2002981. [DOI: 10.1002/aenm.202002981]
- [S7] Dong R, Zheng L, Bai Y, et al. Elucidating the mechanism of fast Na storage kinetics in ether electrolytes for hard carbon anodes. *Adv Mater* 2021;33(36):2008810. [DOI: 10.1002/adma.202008810]
- [S8] Ma M, Cai H, Xu C, et al. Engineering solid electrolyte interface at nano-scale for high-performance hard carbon in sodium-ion batteries. *Adv. Funct. Mater* 2021;31(25):2100278. [DOI: 10.1002/adfm.202100278]
- [S9] Yin X, Zhao Y, Wang X, et al. Modulating the graphitic domains of hard carbons derived from mixed pitch and resin to achieve high rate and stable sodium storage. *Small* 2022;18(5):2105568. [DOI: 10.1002/sml.202105568]
- [S10] Li Y, Kong M, Hu J, Zhou J. Carbon-microcuboid-supported phosphorus-coordinated single atomic copper with ultrahigh content and its abnormal modification to Na storage behaviors. *Adv. Energy Mater.* 2020;10(19):2000400. [DOI: 10.1002/aenm.202000400]

2.

3. <https://www.fda.gov/NewsEvents/Newsroom/PressAnnouncements/ucm574058.htm>

[m](#). [Last accessed on 30 Jan 2021]

- See the following website for more types of writing formats:
- http://www.nlm.nih.gov/bsd/uniform_requirements.html